

## Effect of grain size on the forces governing the dynamic behavior of electrostatically driven powder media

L. M. Salvatierra,<sup>1,2</sup> P. L. Dammig Quiña,<sup>1</sup> L. I. Kovalevski,<sup>1,2</sup> I. M. Irurzun,<sup>1</sup> and E. E. Mola<sup>1,2</sup>

<sup>1</sup>*CCT La Plata-CONICET, Instituto de Investigaciones Fisicoquímicas Teóricas y Aplicadas (INIFTA), Facultad de Ciencias Exactas, Universidad Nacional de La Plata, Diagonal 113 y 64, Código Postal (1900), La Plata, Argentina*

<sup>2</sup>*Facultad de Química e Ingeniería, Pontificia Universidad Católica Argentina, Avenida Pellegrini 3314, Código Postal (2000), Rosario, Argentina*

(Received 25 January 2013; published 25 June 2013)

The aim of this paper is to identify the forces that govern the dynamic behavior of polydisperse granular systems under high electric fields in air media. In a previous paper, we reported the changes in the morphology and dynamics of grain structures under a frequency and amplitude variable voltage and summarized them in a diagram [L. M. Salvatierra *et al.*, *Chem. Phys. Lett.* **481**, 194 (2009)]. In the present article, we investigate the influence of the grain size distribution and the speed of voltage increase during tests. We explain the main transitions observed in the diagram in terms of the change in grain size and the frequency-dependent electrical response, related to electrophoretic and dielectrophoretic interactions.

DOI: [10.1103/PhysRevE.87.062204](https://doi.org/10.1103/PhysRevE.87.062204)

PACS number(s): 45.70.Qj, 81.05.Rm

### I. INTRODUCTION

As a result of their electrical properties, particles less than approximately 1 mm in diameter will suffer the mechanical effects of forces and torques when subjected to electric fields. Closely spaced particles often exhibit strong mutual interactions, cohesion, chaining, and fingering, and therefore, structure and pattern recognitions can be achieved in different liquid or air media [1–11].

When exposed to an electric field, a charged and polarized particle experiences both an electrophoretic force (EP), the product of the particle net charge and the field strength, that is,  $\vec{F}_{EP} = q\vec{E}$ , and a dielectrophoretic force (DEP), the product of the particle dipole moment and the field strength gradient  $\vec{F}_{DEP} = \vec{p} \cdot \nabla \vec{E}$  [2].

The EP force requires a net charged particle, and it can exist in uniform or nonuniform electric fields and ac or dc fields. In a linear ac field, the EP force has a zero time average over a field cycle, and therefore, the average shifting also is zero, although it can cause oscillations in a particle depending on the viscosity of the media.

On the contrary, the DEP force needs a nonuniform field (externally imposed or locally generated). In ac fields, its average yields a nonzero value whose magnitude is the product of the particle volume, the gradient of the time average squared field strength, and the particle polarization at the field frequency.

Granular media consisting of solid grains bigger than 1  $\mu\text{m}$  interact via dissipative short-range contact forces, and the thermal energy is negligible. They remain at rest unless a source of mechanical or electromagnetic energy is applied [3]. In a previous article [1], we experimentally studied microsized granular media (with grain sizes from 1 to 130  $\mu\text{m}$ ) under an ac uniform electric field, and the phase in which there is no movement in the powder was called “precipitated granular solid phase” or Phase I (PI). This regime will extend from zero amplitude of the applied voltage up to a threshold value beyond which the particles start to move. Above that threshold and depending on the frequency and amplitude, the movement of particles has a constructive behavior (forming columnar

or filamentary structures) or a destructive behavior (unstable structures and individual grain movements).

In Ref. [1], both dynamic regimes were experimentally studied, and a diagram was constructed (based on the experimental data obtained in Ref. [1]) showing the voltage amplitude-frequency space regions in which either constructive or destructive behavior was experimentally observed. Figure 1 shows the diagram and some representative pictures of the observed behavior. In Phase II (PII), there is grain pileup and coarsening behavior (constructive). Within this dynamic regime, in Ref. [1], we distinguished three different qualitative zones where each one develops a singular morphology and dynamics: high frequency zone (HFZ), medium frequency zone (MFZ), and low frequency zone (LFZ), respectively. In Phase III (PIII), a completely destructive behavior is observed where individual movements cause instabilities that prevent the growth and cohesion of grains and cause a granular gas. In Ref. [1], the boundaries between phases were determined by visual inspection of the video records performed during the experiments. In each experiment, the voltage is increased from zero at constant rate and frequency, according to the protocol also used in the present article. This procedure avoids hysteretic effects due to the fact that, in the experimental setup, the powder is not physically constrained to a bidimensional space.

In the present paper, we analyze the influence of the weight force on the particle trajectories in Phase III and on the boundaries between dynamics regimes. We do it by studying the influence of the powder grain size, which is a composite salt made up of ammonium monophosphate ( $\text{NH}_4\text{H}_2\text{PO}_4$ ) and ammonium sulfate [ $(\text{NH}_4)_2\text{SO}_4$ ] as in Ref. [1]. Also, we report and discuss the dependence of the boundaries on the speed of voltage increase. By a combination of EP and DEP interactions, we explain the main transitions and dynamic regimes observed in Fig. 1.

### II. EXPERIMENTAL PROCEDURE

The experimental setup used in this paper was similar to the one used in Ref. [1]. A sinusoidal wave was power amplified and was sent to a wideband high-voltage transformer.

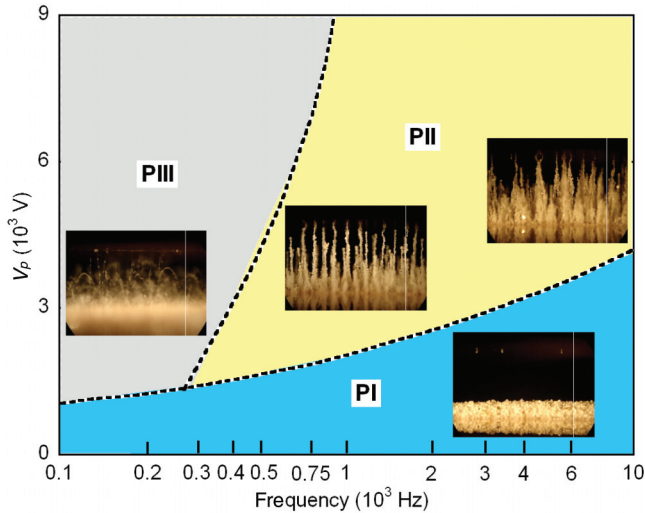


FIG. 1. (Color online) Voltage amplitude-frequency diagram experimentally constructed in Ref. [1]. PI blue (dark gray): precipitated granular solid phase; PII yellow (light gray): constructive behavior; and PIII (gray): destructive behavior. The diagram was constructed by inspection of a video recording of the experiments performed at the explored frequencies (which are labeled on the horizontal axis). In one experiment, the electric field is raised from 0 V at constant rate and at constant frequency. Constructive behavior in Phase II was characterized in Ref. [1] by measuring the maximum height reached by the filaments, normalized to the interelectrode distance  $H_{\max}$  as a function of the applied voltage  $V_p$ .

A Tektronix P6015A high-voltage probe (HVP) with a 75 MHz bandwidth of 20 kV<sub>rms</sub> and a maximum peak-to-peak voltage of 40 kV<sub>pp</sub> was used as a measurement device. The probe was connected to a Tektronix Oscilloscope 1012B of a 1 GS/s and 100 MHz bandwidth online with a PC.

The former 5 mm diameter copper electrodes used in Ref. [1] were replaced by other ones of 36 mm diameter with parallel and polished faces. This change was carefully incorporated to improve the electric field uniformity. As in Ref. [1], the electrodes are joined to a micrometer, one to its fixed part and the other to its movable part, and can be moved maintaining a uniform distance between them (calibrated with micrometric gauges). The distance between the electrode plane parallel faces was adjusted between 0 and 40 mm with an accuracy of 0.01 mm. The dynamic behavior of the granular system was recorded by a digital high-resolution video camera (CCD) together with an optical microscope (OM). The OM looks at the cell horizontally. Additionally, a polymethylmethacrylate cylindrical housing surrounding the electrodes was used to avoid horizontal air currents.

Each sample, consisting of about 5 mg, was placed along the diameter line of a cylindrical cell (perpendicular to the CCD camera). Therefore, the vertical growth of the structure occurred predominantly on a quasi two-dimensional plane, allowing a quasi permanent focused image. The initial length and height of the sample were controlled through a grid in the live view camera software, whereas, the mass (and, therefore, the thickness) was constant. The sample is several grains thick.

The experiment begins with the “aligned sample” placed on the upper face of the lower electrode. The CCD camera

TABLE I. Grain size intervals and nomenclature.

Grain size group	Nomenclature
98–150 $\mu\text{m}$	L: largest grain size group
43–75 $\mu\text{m}$	M: medium grain size group
< 30 $\mu\text{m}$	S: smallest grain size group

records at 30 frames per second. The experiment starts (with a fixed interelectrode distance) by raising the electric field at a constant rate from 0 V and at a constant frequency. The experiment is repeated at different frequencies by cleaning the cell and replacing a new powder sample.

The HV sinusoidal wave is directly monitored through the HVP at the cell itself. Then, the signal is viewed on the oscilloscope’s screen and is recorded and analyzed with the PC. The software used allows us to evaluate the voltage signal and its rise-up rate in real time, triggering it together with the video recording.

As in our previous paper [1], a composite salt made up of 55%  $\text{NH}_4\text{H}_2\text{PO}_4$  and 45%  $(\text{NH}_4)_2\text{SO}_4$  was used. In this paper, the initial grain size distribution was segregated by normalized meshes to obtain narrower grain fractions. Therefore, three different groups of grain sizes (not overlapped) were selected (see Table I).

The distance between electrodes was  $d = 4.13$  mm. The voltage was increased at a constant rate of 0.3 kV/s. Next, for the medium grain size group (M), another two velocities were used to check the effect of the run-up speed: one of them at about 0.6 kV/s (comparable to that used in Ref. [1]) and the other at 0.15 kV/s. The experiments were performed in air (60%–65% air humidity) at normal atmospheric pressure of 1 atm and room temperature (25  $^\circ\text{C}$ ). The powders were stored as received in a sealed container to avoid contact with dust, ambient damp, etc.

### III. EXPERIMENTAL RESULTS

To analyze the influence of the grain size and voltage increase speed on the diagram limits and regions, we first define them by using quantitative criteria. Phase I starts at  $V_p = 0$  and extends up to a  $V_p$  value (which ranges approximately between 1 and 3 kV<sub>p</sub> as the frequency ranges from 300 Hz to 6 kHz) at which grains start to move. We say that a structure starts to grow when it reaches 5% of the interelectrode distance, that is, about two particles of the L group or eight particles of the S group. Therefore, the Phase I-Phase II limit is attained when, at least, one structure starts to grow. Although this criterion involves the movement of several grains, results can be normalized to one grain without changing the main conclusions.

In Phase II, LFZ is the lowest frequency bandwidth at which almost all filaments have a destructive behavior, collapsing, rotating, and vibrating. MFZ is an intermediate bandwidth at which filaments grow continuously as grain by grain strings up to reaching the upper electrode. HFZ is the highest frequency bandwidth where multifilament structures grow with strong horizontal interactions [1].

The Phase II-Phase III limit is reached when no filament can remain stable by two frames (i.e.,  $\frac{2}{30}$  s), and/or we start to distinguish individual particles flying away.

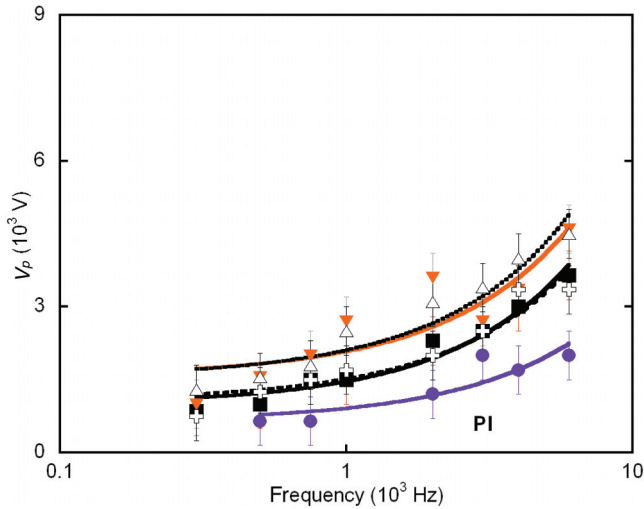


FIG. 2. (Color online) Dependence of the Phase I-Phase II boundary on the grain size and speed of voltage increase. The violet curve (gray) with filled circles, black curve with filled squares, and orange (light gray) curve with filled triangles are S, M, and L groups at 0.3 kV/s, respectively. The dashed black curve with the plus symbol is M at 0.15 kV/s. The dotted black curve with empty triangles is M at 0.6 kV/s.

The Phase I-Phase III limit is reached when particles start to move, but there are no stable filaments with a height of, at least, 5% of the interelectrode distance.

Figure 2 shows the dependence of the Phase I-Phase II boundary on the grain size and voltage increase speed. There is a clear dependence on the grain size, related to the fact that the electrical force must compensate for the particle weight to reach the threshold to allow filament growth (note that this tendency is even more remarkable when normalizing to one grain). There is also a dependence of this limit on the voltage increase speed, even at low frequencies.

Figure 3 shows a series of snapshots where the different morphologies and dynamic regimes of the system can be distinguished at different frequencies and voltages for the three grain size groups. The shift in phase diagram limits and Phase II zones can be observed (e.g., frequency transitions shift to higher values, and voltage transitions move to lower values as the grain size is decreased).

Figures 4(a) and 4(b) show the growth mechanism through a time sequence of one L filament in the LFZ and one structure in the HFZ of Phase II, respectively. In both zones, they grow from the bottom. That is, the entire filament or structure seems to be pulled up from the top electrode (keeping it stretched) and pushed away from the bottom due to neighbor grains that add in the filament base. The growth dynamics in the HFZ of Phase II is characterized by strong horizontal interactions between particles. The result is a multifilament or columnar structure growing as a unique element [see Fig. 4(b)].

The entire Phase II zone was characterized by measuring the maximum height reached by the filaments ( $H_{max}$ ) as a function of the applied voltage ( $V_p$ ). The height of the structures was normalized to the interelectrode distance.

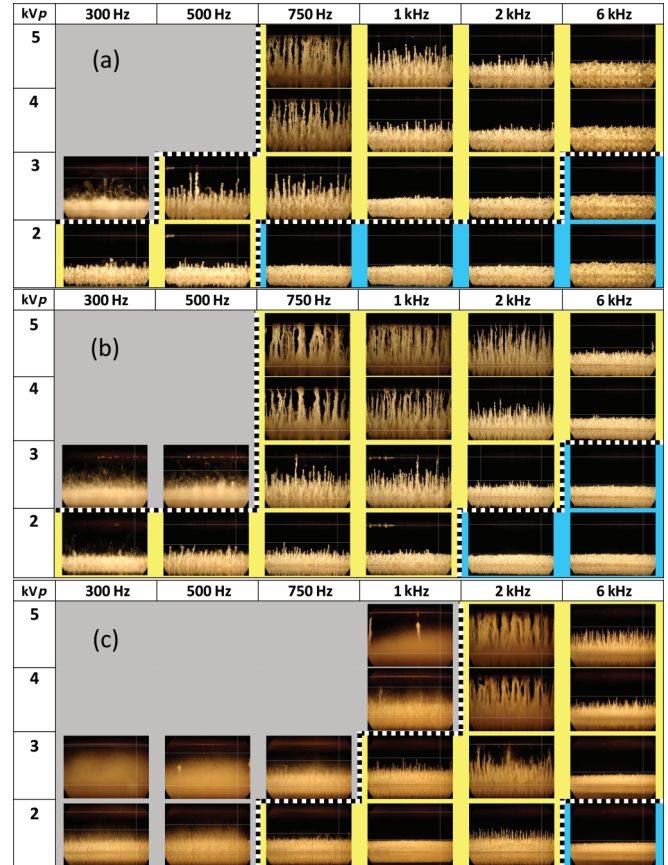


FIG. 3. (Color online) Snapshots showing the different morphologies and dynamic regimes of the system at different frequencies and voltages (typical for PI, PII and PIII) for the three grain size groups. (a) L grain size group, (b) M grain size group, and (c) S grain size group. Dotted lines show the phase limits. Background color code (grayscale code) is the same as in Fig. 1: Phase I is blue (dark gray), Phase II is yellow (light gray), and Phase III is gray. Peak voltages are in kilovolts ( $10^3$  V).

Figure 5(a) shows two major aspects of the behavior observed in Phase II. In the LFZ, the same response does not superimpose in frequency for the L, M, and S groups. This result is consistent with the fact that the grain size intervals in the three groups are not overlapped. For the HFZ, we have plotted isofrequency  $H_{max}$  curves (at 6 kHz)

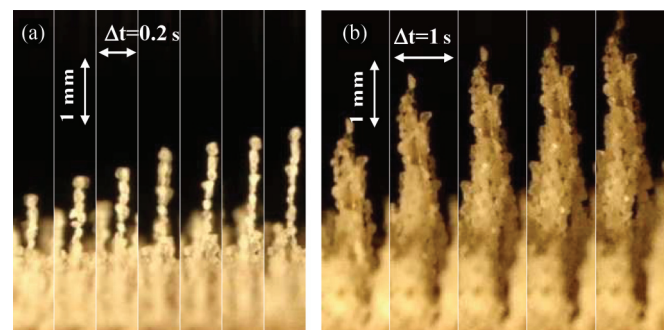


FIG. 4. (Color online) Growth mechanism of: (a) one L filament in the LFZ (sequence at  $\Delta t = 0.2$  s) and (b) one L structure in the HFZ (sequence at  $\Delta t = 1$  s) at 0.3 kV/s.

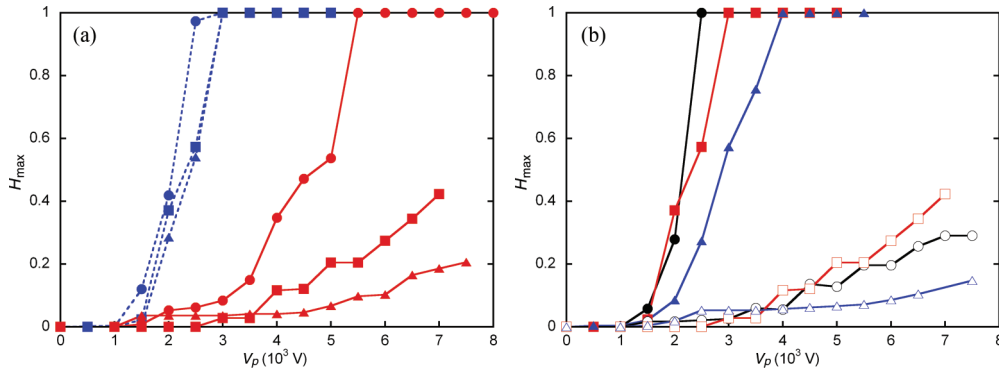


FIG. 5. (Color online) (a) Dependence of  $H_{\max}$  on the applied voltage and grain size. In the LFZ (blue labels and dashed lines), circles: S, 1 kHz; squares: M, 750 Hz; and triangles: L, 500 Hz. In the HFZ (red labels and full lines), circles: S, 6 kHz; squares: M, 6 kHz; and triangles: L, 6 kHz. (b) Dependence of  $H_{\max}$  on the voltage speed increase at 750 Hz (filled labels) and 6 kHz (empty labels), for M particles at 0.15 kV/s (black line and circles), 0.3 kV/s (red line and squares), and 0.6 kV/s (blue line and triangles).

to show the different electrodynamic responses. It is observed that large particles have a slower growth dynamics than that corresponding to M and S groups. For these curves, the voltage was increased at a constant rate of 0.3 kV/s.

Figure 5(b) shows the isofrequency responses at LFZ (750 Hz) and HFZ (6 kHz) at different voltage increase speeds for the M group. There is an inertial effect between the external applied voltage (with an immediate response) and the electromechanical movements (with a time-dependent response).

Figure 6 shows the dynamic regime that takes place in Phase III at lower frequencies. In this dynamic regime, individual grain movements occur. Below 100 Hz, a vertical rain of the whole mass of grains moves through the electrodes

[Fig. 6(a)]. Between 100 and 300 Hz (even up to 750 Hz for the S group), oscillatory trajectories develop in the interelectrode distance [Figs. 6(b)–6(f)]. It must be noted that the oscillation frequency is the same as the field imposed frequency, and it is the ratio between the amount of periods showed by each grain path and the photograph exposure time (controlled from the digital camera); this was verified for all grain size groups,

$$\text{frequency (Hz)} = \text{No. periods/exposure time (s)}. \quad (1)$$

In most cases, grains are ejected from Phase I developing a parabolic trajectory that modulates the sinusoidal oscillation. In particular but not obvious conditions, the grains acquire an average flat levitation with a vertical sinusoidal displacement, assisted or not by a horizontal translation.

#### IV. DISCUSSION

Based on the results presented in Sec. III, we relate the existence of different phases to the competition between the main acting forces: the weight, the EP, and the DEP interactions.

As previously pointed out, when exposed to an electric field, a charged and polarized particle (i.e., a particle with a nonuniform charge distribution) experiences the action of an EP force, the product of the net particle charge and the field strength, and a DEP force, the product of the particle dipole moment and the field strength gradient [2,12–14].

In Phase I, the weight force  $mg$  on each grain clearly dominates over the EP and DEP interactions (see Fig. 1). In addition, one should consider an average term involving all the static short-range forces, which should also be exceeded to allow movement (i.e., friction forces, surface hygroscopicity, submicron forces, etc.) and depend on the particle size and shape.

EP forces appear when  $V_p > 0$  and charges are promoted inside this precipitated granular phase on the bottom electrode. DEP forces can also develop only due to polarized particles and local field nonuniformities originated by the rugosity of the sample surface as the imposed external field is fairly uniform. The local nonuniformities occur in any direction inside Phase I, some of them, strong enough to move a grain over others.

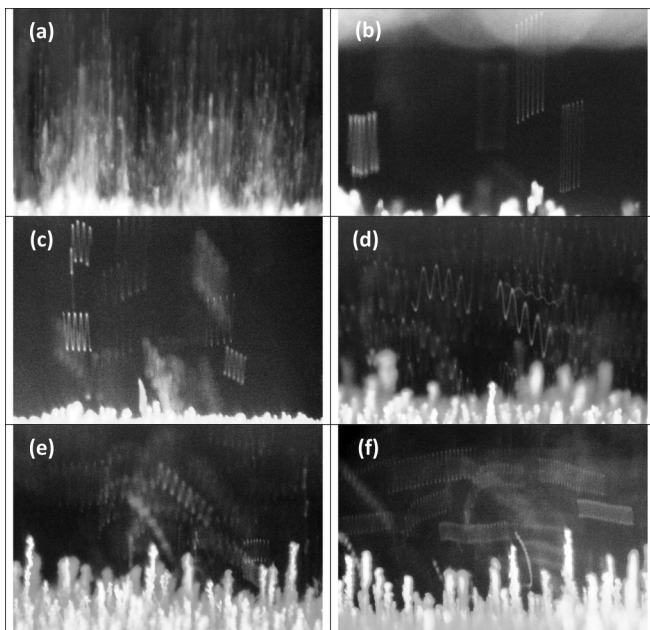


FIG. 6. Photographs of trajectories at different frequencies in Phase III. (a)  $100 \text{ Hz} \times \frac{1}{15} \text{ s} = 6.66$  cycles, (b)  $200 \text{ Hz} \times \frac{1}{30} \text{ s} = 6.66$  cycles, (c)  $300 \text{ Hz} \times \frac{1}{60} \text{ s} = 5$  cycles, (d)  $300 \text{ Hz} \times \frac{1}{60} \text{ s} = 5$  cycles, (e)  $500 \text{ Hz} \times \frac{1}{60} \text{ s} = 8.33$  cycles, and (f)  $750 \text{ Hz} \times \frac{1}{30} \text{ s} = 25$  cycles.

Figure 2 shows that the Phase I-Phase II boundary is reached at higher voltages (at a fixed frequency) when the particle size or volume ( $\propto R^3$ ) and, therefore, weight are increased, dominating over area-dependent contact forces. On the other hand, the fact that this upper limit of Phase I depends on the rate of increase in potential might indicate the existence of a delay between the external applied voltage and the electromechanical movements.

Phase III is observed when, at a fixed voltage  $V_p$ , the frequency is low enough to permit vertical distance travel (amplitude) in a half cycle greater than a grain diameter. Before the reversal of the field polarity, the grain has no more contact with its neighbors, so it can be ejected at high speeds.

When a particle having a net charge  $q$  is ejected from Phase I in the bottom electrode, it is under an EP force ( $F_{EP}$ ) given by

$$F_{EP} = qE, \quad (2)$$

where the  $F_{EP}$  has the vertical direction of  $E$  in the  $z$  axis and  $E = E_0 \sin(2\pi ft)$ . Therefore, the net force in a levitated or flying charged particle is as follows:

$$F_N = F_{EP} - mg, \quad (3)$$

where  $mg$  is the weight force. Since the field strength is  $E = V/d$ , where  $V$  is the applied potential in volts and  $d$  is the interelectrode distance, Eq. (3) can be written in the following way:

$$m\ddot{z} = \frac{V_p}{d}q \sin(2\pi ft) - mg, \quad (4a)$$

$$\ddot{z} = \frac{V_p}{d} \frac{q}{m} \sin(2\pi ft) - g. \quad (4b)$$

The general solution of Eq. (4b) is

$$z(t) = -C \sin(2\pi ft) - \frac{1}{2}gt^2 + v_{z0}t + z_0, \quad (5)$$

where  $v_{z0}$  is the particle initial velocity along the  $z$  axis and  $z_0$  is its position at  $t = 0$ . The constant  $C$  is obtained by calculating the time second derivative of Eq. (5),

$$\ddot{z} = 4\pi^2 f^2 C \sin(2\pi ft) - g. \quad (6)$$

Comparing Eqs. (4b) and (6),

$$C = \frac{V_p}{4\pi^2 f^2 d} \frac{q}{m}. \quad (7)$$

Therefore, the equation of movement of our charged particle in an oscillating electric field will be

$$z(t) = A_0 \sin(2\pi ft) - \frac{1}{2}gt^2 + v_{z0}t + z_0, \quad (8)$$

where  $A_0 = \frac{3}{16} \frac{V_p}{\pi^3 f^2 d} \frac{q}{\rho R^3}$ ,  $m = \frac{4}{3}\pi R^3 \rho$ , and  $\rho$  is the substance density.

If we consider that the accumulation of charge on a dielectric particle is a surface process,  $q$  can be expressed as  $q = 4\pi R^2 \phi$ , where  $\phi$  is the surface charge density and the amplitude can be rewritten as

$$A_0 = \frac{3}{4} \frac{V_p}{\pi^2 f^2 d} \frac{\phi}{\rho R}. \quad (9)$$

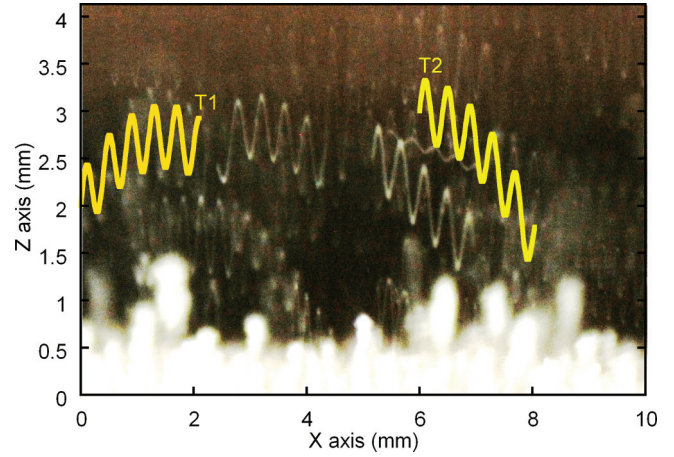


FIG. 7. (Color online) Phase III, Fig. 6(d) with modeled trajectories.  $\Delta t =$  experimental time =  $1/30$  s,  $f = 300$  Hz,  $V_p = 1000$  V,  $2R = 30 \mu\text{m}$ ,  $d = 4.13$  mm,  $\phi = 4.35 \times 10^{-5}$  C/m<sup>2</sup>. T1:  $(x_0, z_0) = (0, 2) \times 10^{-3}$  m,  $v_{z0} = 0.12$ ,  $v_x = 0.12$  m/s. T2:  $(x_0, z_0) = (6, 3) \times 10^{-3}$  m,  $v_{z0} = 0$ ,  $v_x = 0.12$  m/s.

By measuring  $A_0$  in trajectories of known size particles at different values of  $V_p$  and  $f$ , a value of  $\phi = 4.35 \times 10^{-5}$  C/m<sup>2</sup> was obtained.

In Fig. 7, we plotted the predicted trajectories from Eq. (8) for a given set of parameters into Fig. 6(d) and a surface charge density  $\phi = 4.35 \times 10^{-5}$  C/m<sup>2</sup>.

Figure 8 shows the dependence of  $V_p$  against the frequency predicted by the model to move a grain an amplitude of  $A_0 = 2R$ . This is also in agreement with the observed experimental behavior (i.e., the Phase III-Phase II limit shifts to higher voltages or higher frequencies when the grain size is decreased).

The evidence given by using Eq. (8) in Fig. 7 tells us that the EP force dominates the system for the ejected grains. The simulated paths are consistent with the experimental ones. Initial conditions at  $t = 0$  will depend on how the particle is ejected. Deviations from parabolic paths might be explained

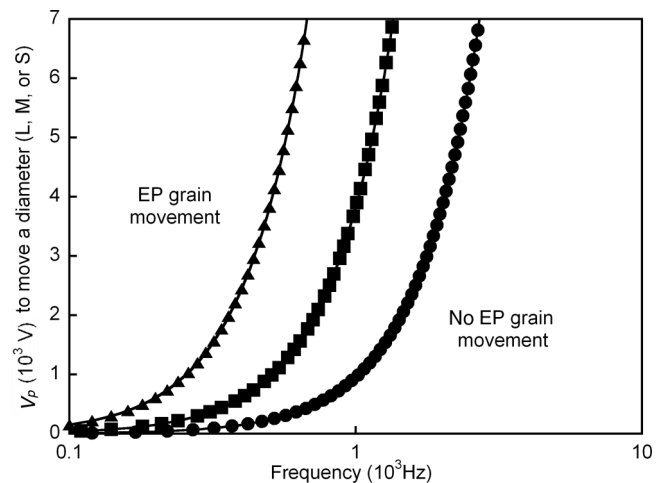


FIG. 8.  $V_p$  vs  $f$ , needed to move a grain S (circles), M (squares), or L (triangles) a distance of  $A_0 = 2R$  due to an EP force [see Eq. (8) with  $d = 4.13$  mm].

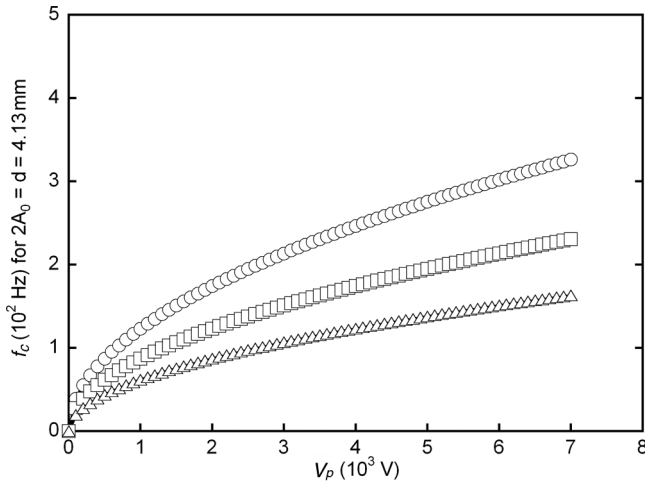


FIG. 9. Critical frequency  $f_c$  against  $V_p$  to oscillate a grain S (circles), M (squares), or L (triangles) a  $z$  distance of  $2A_0 = d = 4.13$  mm, where  $d$  is the interelectrode distance.

by local instabilities and fluctuations in the air mass as well as interactions with other nearby particles.

The DEP force should not be acting on particles flying in a uniform field far away from others. However, self-induced DEP forces can be acting in any direction inside Phase I and might be co-responsible for local movements and the ejecting mechanisms.

As  $A_0$  grows with  $1/f^2$ , if a flying particle reaches the counterelectrode in a time less than a half cycle, then it falls down, resting on the bottom electrode. A second wave impact was experimentally observed in the next half cycle. Both are triggered by the maximum and minimum values of  $V_p$ . This effect might be indicating that positively and negatively charged grains might be present at the same time in these samples.

When the frequency is increased, the particles have no time gap resting on the bottom electrode, awaiting a new maximum or minimum, and they are continuously in movement as a constant rain shower [Fig. 6(a)].

Let  $f_c$  be the frequency value at which  $2A_0 = d$  [see Eq. (10)]. Above this critical frequency, which is a function of  $V_p$ ,  $R^3$ , and  $d$  (see Fig. 9), trajectories have amplitudes less than  $d$  as in Figs. 6(b)–6(f).

As the frequency increases, the movement of the particles is restricted to shortened amplitudes, and Phase II starts. Note that the Phase III-Phase II limit also depends on both the grain size and the electric field amplitude (see Fig. 8). Going to higher frequencies, the EP force vanishes, and polarization effects start to dominate the system.

According to Ref. [2], two closely polarized dielectric particles tend to attract each other when they are oriented with their line of centers parallel to a uniform applied electric field  $\vec{E}_0$  and repel each other when they are aligned perpendicular to it (side by side), no matter the sign of Clausius-Mossotti function ( $K$ ). This can be demonstrated with a single dipole-dipole approximation [2] where the resulting net effective dipole moment of these two or more particles is enhanced when the chain is aligned parallel to the field and  $K > 0$ . Therefore, chain formation in a uniform electric field is

thermodynamically favorable if no DEP force is externally imposed by a nonuniform field configuration. This mechanism can be generalized to charged particles with a nonuniform charge distribution.

In the LFZ of Phase II, polarized and/or charged particles can be aligned by the electric field. There are large fluctuations due to variations in the size of the particles within each group: Small particles might move distances longer than their diameters producing mechanical destabilization of the filament. In a hypothetical experiment where all grains have the same  $R^3$ , there would be a discrete transition (in frequency) between gas and filaments.

As can be seen from Fig. 4, filaments in Fig. 4(a) or structures in Fig. 4(b) grow by adding one or more grains from the base and not from the top. We notice that, once some filaments or structures start to grow, there is the above-mentioned “enhancing effect” of the net effective dipolar or multipolar moment, which favors the growth of these filaments instead of the initiation of closely new ones.

In the HFZ, the powder starts to respond mechanically as a set of polarized and/or charged particles, which can interact attractively and can form aggregates that grow (such as pine trees) toward the upper electrode. The accumulation of material in these structures is further from the base [see Fig. 4(b)]. However, the interaction forces between individual filaments dominate the dynamics of the system; often, a filament can be seen climbing over another. The growth dynamics (curve of  $H_{\max}$ ) is very dependent on the grain size, being slower for large particles than for medium and small ones. Note the large number of particles involved per structure in this zone.

## V. CONCLUSIONS

In this paper, we studied the dynamic behavior of a composite inorganic salt subjected to a uniform high electric field at different voltage amplitudes and frequencies. We studied the effect of the grain size and the rate of increase in potential and related the dynamic behavior in different phases and limit shifting with electrophoretic and dielectrophoretic mechanisms. Thus, in Phase I, the weight of the particles dominates over the electrical forces, which becomes dominant in Phase III. In this phase, the particle movements follow the electric field fluctuations. Phase II begins at frequencies where polarization forces (dipolar contribution) become dominant and particles can be aligned to form a filament in the direction of the electric field. At higher frequencies, a cooperative alignment is possible, and the particles are added to maximize the attractive interactions between them. Then, they form aggregates that grow toward the upper electrode.

To elucidate the origin of the charge on the particles, several additional experiments are being performed, and results will be presented in a forthcoming paper. Measurements at very low frequencies suggest that both positively and negatively charged particles are present in the sample. By adding dielectric barriers between the samples on both electrodes, we realize that the charges are not injected from the electrodes. The charge may initially be present in the sample or may be the result of the particle-particle friction flow. Attempts to neutralize or uniform the initial charge in the sample as well as impedance

analyses to electrically characterize the samples are being made.

Studies have also been performed with glass beads with similar sizes [15]. Experiments suggest that the grain geometry has an important effect on the dynamic behavior of the system, mainly at intermediate values of frequency and voltage (LFZ of Phase II). Although the spherical geometry implies that only normal contact forces act between particles, irregular grain contours introduce steric limitations that are important

to explain the structure growth mechanism in the LFZ-II. A comparison between spherical and irregular grains will be presented elsewhere.

#### ACKNOWLEDGMENTS

This research project was financially supported by the National Research Council of Argentina (CONICET), the National University of La Plata, and the ANPCyT.

- 
- [1] L. M. Salvatierra, O. L. Cortés Bracho, P. L. Dammig Quiña, I. M. Irurzun, and E. E. Mola, *Chem. Phys. Lett.* **481**, 194 (2009).
  - [2] T. Jones, *Electromechanics of Particles* (Cambridge University Press, Cambridge, UK, 1995).
  - [3] A. J. Liu and S. R. Nagel, *Nature (London)* **396**, 21 (1998).
  - [4] H. M. Jaeger, S. R. Nagel, and R. P. Behringer, *Rev. Mod. Phys.* **68**, 1259 (1996).
  - [5] L. P. Kadanoff, *Rev. Mod. Phys.* **71**, 435 (1999).
  - [6] M. V. Sapozhnikov, A. Peleg, B. Meerson, I. S. Aranson, and K. L. Kohlstedt, *Phys. Rev. E* **71**, 011307 (2005).
  - [7] I. S. Aranson and L. S. Tsimring, *Rev. Mod. Phys.* **78**, 641 (2006).
  - [8] I. S. Aranson, D. Blair, V. A. Kalatsky, G. W. Crabtree, W.-K. Kwok, V. M. Vinokur, and U. Welp, *Phys. Rev. Lett.* **84**, 3306 (2000).
  - [9] M. V. Sapozhnikov, I. S. Aranson, and J. S. Olafsen, *Phys. Rev. E* **67**, 010302 (2003).
  - [10] M. Belkin, A. Snezhko, I. S. Aranson, and W. K. Kwok, *Phys. Rev. Lett.* **99**, 158301 (2007).
  - [11] I. S. Aranson and M. V. Sapozhnikov, *Phys. Rev. Lett.* **92**, 234301 (2004).
  - [12] F. A. Sauer, in *Interactions between Electromagnetic Fields and Cells*, edited by A. Chiabrera, C. Nicolini, and H. P. Schwan (Plenum, New York, 1985), p. 181.
  - [13] F. A. Sauer and R. W. Schlögl, in *Interactions between Electromagnetic Fields and Cells*, edited by A. Chiabrera, C. Nicolini, and H. P. Schwan (Plenum, New York, 1985), p. 203.
  - [14] W. Y. Fowlkes and K. S. Robinson, in *Particles on Surfaces: Detection, Adhesion and Removal*, edited by K. L. Mittal (Plenum, New York, 1988), p. 143.
  - [15] G. Perez-Mitta, Undergraduate thesis, University of La Plata, 2013.